Two-photon interference using background-free quantum frequency conversion of single photons from a semiconductor quantum dot

Serkan Ates,[1,2,*] Imad Agha,[1,2] Angelo Gulinatti,[3] Ivan Rech,[3]
Matthew T. Rakher,[1] Antonio Badolato,[4] and Kartik Srinivasan[1,†]

[1] *Center for Nanoscale Science and Technology, National Institute of Standards and Technology, Gaithersburg, MD 20899, USA*
[2] *Maryland NanoCenter, University of Maryland, College Park, MD*
[3] *Politecnico di Milano, Dipartimento di Electronica e Informazione, Piazza da Vinci 32, 20133 Milano, Italy*
[4] *Department of Physics and Astronomy, University of Rochester, Rochester, New York 14627, USA*

(Dated: February 20, 2022)

We show that quantum frequency conversion (QFC) can overcome the spectral distinguishability common to inhomogeneously broadened solid-state quantum emitters. QFC is implemented by combining single photons from an InAs quantum dot (QD) at 980 nm with a 1550 nm pump laser in a periodically-poled lithium niobate (PPLN) waveguide to generate photons at 600 nm with a signal-to-background ratio exceeding 100:1. Photon correlation and two-photon interference measurements confirm that both the single photon character and wavepacket interference of individual QD states are preserved during frequency conversion. Finally, we convert two spectrally separate QD transitions to the same wavelength in a single PPLN waveguide and show that the resulting field exhibits non-classical two-photon interference.

Quantum frequency conversion (QFC) [1] is a potentially crucial resource in interfacing photonic quantum systems operating at disparate frequencies. Such a hybrid quantum system could, for example, combine robust and stable quantum light sources based on solid-state emitters [2] with broadband quantum memories based on dense atomic ensembles [3] to enable entanglement distribution in a long-distance quantum network [4]. QFC has been enabled by the development of high-efficiency frequency conversion techniques [5, 6], and been demonstrated in experiments showing that the quantum character of a light field was preserved during the process [7–13]. It can be particularly valuable for solid-state quantum emitters, as prominent systems like semiconductor quantum dots [2] and nitrogen vacancy centers in diamond [14] exhibit significant inhomogeneous broadening. Thus, although these systems are in principle scalable, applications which require identical quantum light sources need a mechanism to bring spectrally disparate sources into resonance [15–19]. Unlike previous demonstrations, in which techniques such as strain/optical/electric fields were applied, QFC can fulfill this role [20] without requiring direct modification of the sources themselves.

Here, we demonstrate nearly background-free QFC, which we use to enable experiments examining photon statistics and two-photon interference of single photons from a semiconductor quantum dot. Compared to previous telecommunications (1300 nm) to visible (710 nm) conversion [10], we work with quantum dots (QDs) emitting in the well-studied 900 nm to 1000 nm wavelength range [2], and convert their single photon emission to 600 nm, a wavelength region in which Si single photon avalanche diodes (SPADs) offer a combination of quantum efficiency and timing resolution that is currently unavailable in the 980 nm band [21, 22]. Using a much wider wavelength separation between signal and pump photons improves the signal-to-background level by about two orders of magnitude with respect to Ref. 10. Measurements of photon statistics and two-photon interference before and after conversion indicate no degradation in purity or wavepacket overlap of the single photon stream due to the frequency conversion process. Finally, we show that two spectrally separate transitions of a QD can be converted to the same wavelength in a single PPLN waveguide, and present initial measurements demonstrating two-photon interference of these frequency-converted photons. This represents a first step towards a resource-efficient approach in which a single nonlinear crystal acts as a QFC interface that generates indistinguishable photons from different solid-state sources [23].

The basic experimental system is depicted in Fig. 1(a) and described in detail in the Supplemental Information [24]. Our single photon source is an InAs QD in a fiber-coupled, GaAs microdisk optical cavity [25] excited by a continuous wave (cw) or pulsed (50 MHz repetition rate, 50 ps pulse width) 780 nm laser diode. Spectrally isolated emission from the QD can be studied in the 980 nm band through photon correlation and two-photon interference (Hong-Ou-Mandel [26]) measurements, or else sent to the frequency conversion setup. Frequency conversion is done by combining a strong, tunable 1550 nm pump laser with the 980 nm QD signal and coupling them into a PPLN waveguide. The 600 nm converted signal is spectrally isolated and sent into either a second photon correlation or Hong-Ou-Mandel apparatus, to study the photon statistics and two-photon interference after frequency conversion.

We characterize the frequency conversion setup [24] using an attenuated (≈ 30 fW) 980 nm band laser. First, we measure the quasi-phase-matching bandwidth of the PPLN waveguide, and find that it follows the expected sinc^2 response [5] with an inferred bandwidth in the

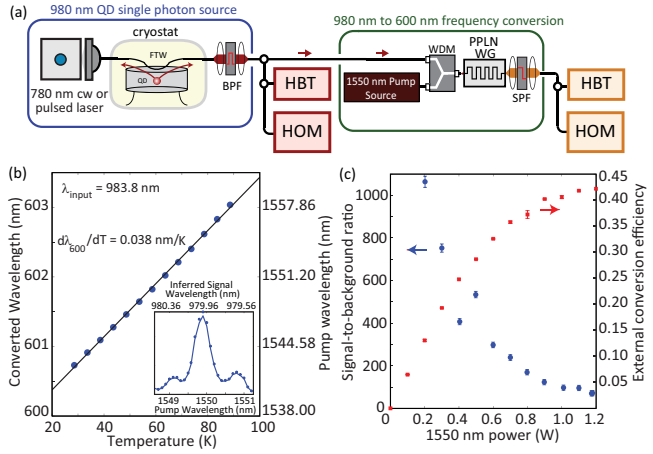

FIG. 1. (a) Experimental setup used within this work [24]. HBT = Hanbury-Brown and Twiss setup; HOM = Hong-Ou-Mandel interferometer. (b) Converted 600 nm band wavelength vs. PPLN waveguide temperature. The inset shows the quasi-phase-matching response of the PPLN waveguide. (c) Signal-to-background ratio (left y-axis, blue points) and external conversion efficiency (right y-axis, red points) as a function of 1550 nm pump power. The external conversion efficiency includes all losses in the system.

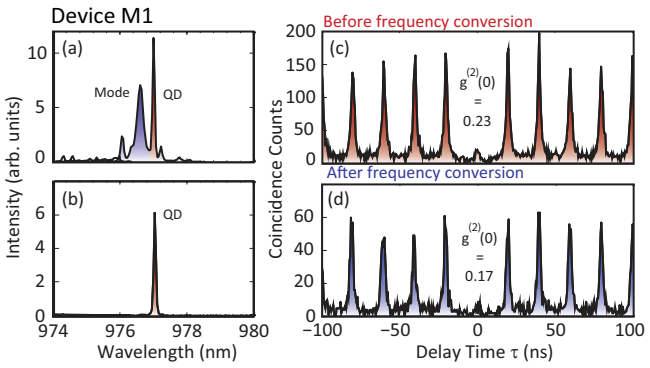

FIG. 2. (a) Low-temperature μ-PL spectrum of device M1. Bright QD emission and cavity mode emission are visible around 977 nm. (b) Spectrum of QD emission filtered by a volume Bragg grating. (c)-(d) Second-order autocorrelation function measurements performed on the QD emission line before and after frequency conversion.

980 nm band of ≈ 0.20 nm (inset of Fig. 1(b)). Next, we study how the frequency converted wavelength changes with PPLN waveguide temperature, which influences phase-matching through thermo-optic and thermal expansion contributions. The resulting plot in Fig. 1(b) indicates that the output wavelength can be tuned by ≈ 2 nm. We have also found that signals between 970 nm and >995 nm can be converted (>35 % external conversion efficiency) by appropriately adjusting the 1550 nm wavelength and PPLN waveguide temperature. This covers the s-shell emission range of the QD ensemble, and means that QDs emitting at different wavelengths (unavoidable due to size/shape/composition dispersion during growth) can be converted to the same wavelength.

Ideally, QFC should avoid generating noise photons that are spectrally unresolvable from the frequency-converted quantum state. Sum- and difference-frequency generation in $\chi^{(2)}$ materials are background-free in principle [1], meaning that signal photons are directly converted to idler photons without amplifying vacuum fluctuations. However, other processes, such as frequency conversion of broadband Raman-scattered pump photons, may still be a source of noise, as observed in experiments using PPLN waveguides [27]. To quantify this, the signal-to-background ratio of the converted signal is measured, and reveals the fraction of converted photons originating from the signal rather than noise processes. In previous work [10], the signal-to-background was limited to 7:1, and though use of a pulsed pump removed temporally distinguishable background noise [28], it did not improve the signal-to-background level. While better spectral filtering provides improvement ($>$ 10:1 signal-to-background was reported recently [13]), it is perhaps more desirable to suppress the noise source, for example, by increasing the separation between the signal and red-detuned pump [27, 29, 30]. Here, our pump-signal separation is nearly 600 nm, suggesting potentially significant improvement.

To test this, we measure (Fig. 1(c)) the signal-to-background level by spectrally isolating the 600 nm conversion band [24] and comparing the detected counts on the SPAD with and without the presence of the 980 nm band signal (the SPAD dark count rate of ≈ 50 s^{-1} is subtracted to give a detector-independent metric). We also plot the external conversion efficiency, which includes all PPLN input/output coupling, free-space transmission, and spectral filtering losses (detector quantum efficiency is not included). The signal-to-background level remains above 100 for all but the highest 1550 nm pump powers, where the conversion efficiency has begun to roll off. For the experiments that follow, we operate with a 35 % to 40 % external conversion efficiency and a signal-to-background level $>$100. As the PPLN incoupling efficiency is ≈ 60 %, and the transmission through all optics after the PPLN waveguide is ≈ 80 %, the internal conversion efficiency in the PPLN waveguide is >70 %.

We now present measurements combining frequency conversion with QD-based single photon sources. We study three devices, M1, M2, and M3, under pulsed and cw excitation conditions. Pulsed measurements are a convenient way to judge the temporal distribution of noise photons produced in the conversion process. Figure 2(a) shows a low temperature (T = 10 K) microphotoluminescence (μ-PL) spectrum of device M1 under 780 nm pulsed excitation. A bright single QD exciton line at 977.04 nm is visible next to a cavity mode at 976.65 nm. The QD emission line was spectrally filtered

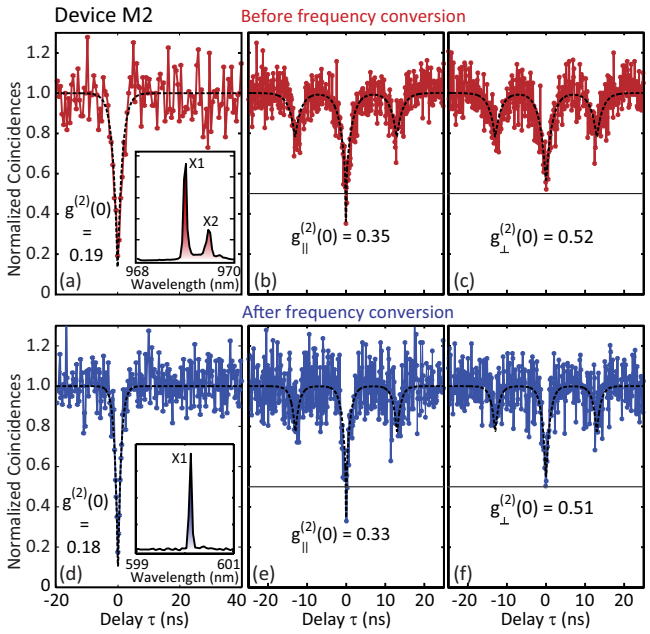

FIG. 3. (a) Auto-correlation of the X1 emission line from device M2 under cw excitation (μ-PL spectrum inset). (b) and (c) Two-photon interference of the X1 line under parallel and orthogonal polarization configurations of the interferometer arms, respectively. (d) Auto-correlation of the X1 line after frequency conversion (frequency converted spectrum inset). (e) and (f) Two-photon interference of the frequency converted X1 line under parallel and orthogonal polarization configurations of the interferometer arms, respectively. The dashed lines are fits to the experimental data [24], and the solid line marks $g^{(2)}(0) = 0.5$ level.

by a volume Bragg grating whose output was coupled to a single mode fiber (Fig. 2(b) shows the filtered QD emission). Before performing frequency conversion, this filtered emission was directed to an HBT setup for photon correlation measurements, the results of which are shown in Fig. 2(c). A strong suppression of the peak at zero time delay to a value of $g^{(2)}(0) = 0.23 \pm 0.04 < 0.5$ is observed. Next, the filtered PL was sent to the frequency conversion setup, and an auto-correlation measurement was performed on the QD emission after it was converted to 600 nm. As shown in Fig. 2(d), the single-photon nature of the QD emission was preserved during the conversion process, proven by the value of $g^{(2)}(0) = 0.17 \pm 0.03$, and no excess noise from the frequency conversion process was observed. In fact, the additional spectral filtering provided by the quasi-phase-matching process is the likely cause of the reduction in $g^{(2)}(0)$ after frequency conversion.

Similar measurements were performed under cw excitation on device M2, whose PL spectrum is shown in the inset to Fig. 3(a). Two bright excitonic lines X1 and X2 are observed on top of a broad cavity mode around 969.5 nm. Figures 3(a) and (d) show auto-correlation measurements performed on the filtered X1 line before and after frequency conversion to 600 nm, respectively (See inset of Fig. 3 (d) for the PL spectrum of converted signal). Antibunching dips in both figures ($g^{(2)}_{\text{before}}(0) = 0.19 \pm 0.01$ and $g^{(2)}_{\text{after}}(0) = 0.18 \pm 0.02$) again show that the single photon nature of QD emission is conserved through the frequency conversion process.

In many cases, both single photon purity and single photon indistinguishability [31] are important. At the heart of indistinguishability measurements is two-photon interference [26], which we now show is preserved in our frequency conversion process. Two-photon interference under cw excitation was performed using a fiber-based Mach-Zehnder interferometer [24] similar to Refs. [32, 33], where one interferometer arm contains a 12.5 ns delay and a polarization rotator. Rotating the polarization of photons from this arm that are incident on the second beamsplitter of the Mach-Zehnder reveals the effect of interference on the photon correlations. In the orthogonal polarization configuration, the interferometer arms are distinguishable and $g^{(2)}_{\perp}(0) = 0.5$ for a pure single photon source. On the other hand, in the parallel polarization configuration, one expects interference between the photons within their coherence time, leading to $g^{(2)}_{\parallel}(0) = 0$. Figures 3(b) and (c) show the results of experiments on the X1 emission before frequency conversion. The antibunching values are $g^{(2)}_{\parallel}(0) = 0.35 \pm 0.03$ and $g^{(2)}_{\perp}(0) = 0.52 \pm 0.04$, yielding the visibility of two-photon interference as $\mathrm{V} = (g^{(2)}_{\perp}(0) - g^{(2)}_{\parallel}(0))/g^{(2)}_{\perp}(0) = 0.33 \pm 0.08$. The deviation from the ideal value of $\mathrm{V} = 1$ stems from the non-zero value of $g^{(2)}(0)$ (Fig.3(a)) and the time resolution of the photon correlation setup that is on the order of the coherence time ($\approx$ 100 ps) of the QD emission [33]. The same experiments were performed on the X1 emission line after frequency conversion, and Figs. 3(e) and (f) show the results for parallel and orthogonal polarization configurations, respectively ($g^{(2)}_{\parallel}(0) = 0.33 \pm 0.03$, $g^{(2)}_{\perp}(0) = 0.51 \pm 0.05$). Due to the conservation of the QD coherence time during the frequency conversion process, we observed a similar two-photon interference visibility $\mathrm{V} = 0.35 \pm 0.09$ at 600 nm.

As discussed earlier, a wide wavelength range of QD emission within the 980 nm band can be efficiently converted to 600 nm by controlling the temperature of the PPLN waveguide and the wavelength of the 1550 nm pump laser. This enables the conversion of well-separated emission lines to the same wavelength at 600 nm. To demonstrate this, both bright emission lines X1 and X2 from device M2 (μ-PL spectrum repeated in Fig. 4(a)) are directed to the frequency conversion setup [24], together with two 1550 nm cw pump lasers whose wavelengths are optimized for efficient conversion of the two 980 nm band signals (which are separated by ≈ 0.5 nm). Figure 4(c) shows the PL spectrum of the total converted

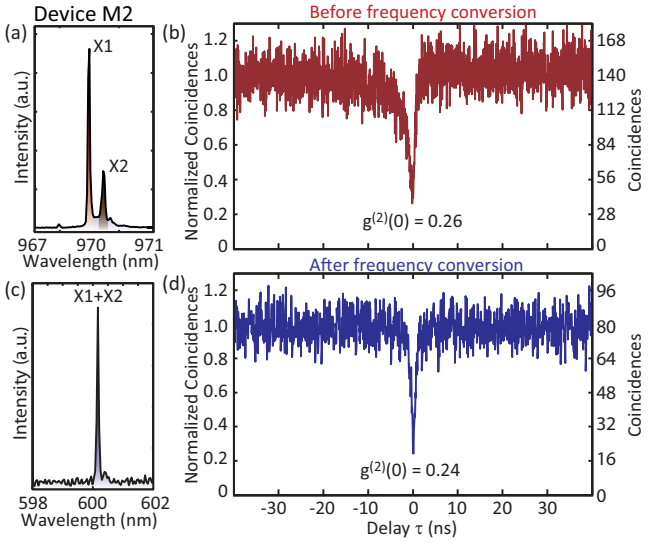

FIG. 4. (a) μ-PL spectrum of device M2 under above-band excitation. (b) Cross-correlation measurement performed on X1 and X2 emission lines. (c) PL spectrum after both lines are converted to the same wavelength at 600 nm. (d) Autocorrelation measurement of the combined frequency converted signal of X1 and X2.

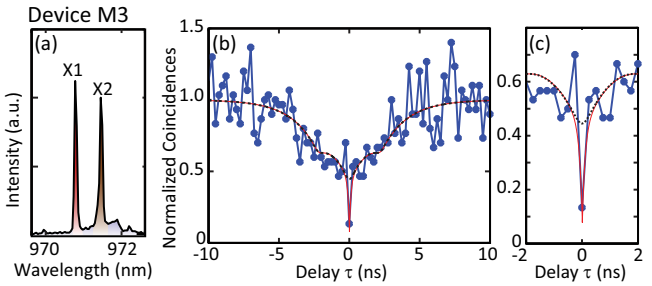

FIG. 5. (a) μ-PL spectrum of device M3 under above-band excitation. Two bright excitonic emission lines (named X1 and X2) are observed with nearly equal intensity. (b) Two-photon interference of the combined X1 and X2 signal after both lines are frequency converted to the same wavelength at 600 nm and measured in the parallel polarization configuration. (c) Zoom-in near the central dip of part (b). The solid red line is a fit to the data, while the black dashed line corresponds to the orthogonal polarization configuration. $g_{\parallel}^{(2)}(0) < g_{\perp}^{(2)}(0)$ is due to the two-photon interference effect.

signal at 600 nm, where the converted signals of the individual X1 and X2 lines are spectrally overlapped (within the spectrometer's resolution $\approx 40\,\mu$eV).

To better understand the nature of the measured emission lines, a cross-correlation measurement was performed before frequency conversion, where the spectrally filtered X1 and X2 lines were sent to the stop and start channels of the HBT setup, respectively. As shown in Fig. 4(b), a strong asymmetric antibunching dip is observed with $g^{(2)}(0) = 0.26 \pm 0.02$. The antibunching shows that both emission lines originate from the same QD, while the asymmetry is related to the radiative dynamics within the QD. The faster recovery time for $\tau > 0$ can be explained if X1 and X2 arise from neutral and charged excitonic emission, respectively [34]. This effect arises because emission of the charged exciton X2 leaves the QD with a single charge, so that subsequent emission in the neutral exciton state X1 requires capture of only a single (opposite) charge. This yields a much faster recovery time than that needed to obtain three charges in the QD, which sets the recovery time for $\tau < 0$.

Next, autocorrelation was performed on the total converted signal at 600 nm, the result of which is shown in Fig. 4(d). As expected, a strong antibunching dip with $g^{(2)}(0) = 0.24 \pm 0.02$ is observed. In contrast to the cross-correlation measurement before conversion, the antibunching dip now has a symmetric shape. This arises from the fact that both QD states were converted within a single PPLN waveguide, so that in the subsequent HBT measurement, the start and stop channels are fed by the same signal at 600 nm, which was composed of both X1 and X2 emission lines. This mixing of the signals going into the start and stop channels removes the asymmetry observed in the cross-correlation measurement before frequency conversion (Fig. 4(b)).

Finally, we consider two-photon interference from two spectrally distinct QD transitions, as a preliminary step towards using QFC to generate indistinguishable photons from different QDs, which has recently been shown through direct tuning of one of the QD transitions [15, 16]. We work with device M3, whose spectrum is shown in Fig. 5(a), and which was chosen because the two excitonic states X1 and X2 have relatively similar intensities. Cross-correlation measurements [24] similar to those described above were performed to confirm that both states come from the same QD. After this, the two states were converted to the same 600 nm wavelength as above, and the combined frequency converted signal was sent into a Mach-Zehnder interferometer similar to that used earlier. Data from the parallel polarization configuration is shown in Fig. 5(b)-(c), where the effect of interference on the photon correlations is seen in the narrow dip at zero time delay, which reaches a value of $g_{\parallel}^{(2)}(0) = 0.13 \pm 0.04$. In comparison, the minimum calculated value (assuming a pure single photon source and infinite timing resolution) for the orthogonal (non-interfering) polarization configuration in our setup [24] is $g_{\perp}^{(2)}(0) = 0.36$. This is smaller than the typical value of 0.5 [33] due to the delay $\Delta\tau$=2.2 ns between the interferometer arms, which is comparable to the average radiative lifetime T_1=1.7 ns of the two states. Taking into account the non-zero value $g^{(2)}(0) = 0.10$ and the finite timing resolution of the setup, $g_{\perp}^{(2)}(0) = 0.45 \pm 0.04$ is estimated [24], far exceeding the measured value $g_{\parallel}^{(2)}(0) = 0.13 \pm 0.04$, and

indicating the significant effect of two-photon interference from the two frequency-converted QD states.

In summary, we have demonstrated background-free quantum frequency conversion of single photons emitted from a quantum dot. Photons at 980 nm are converted to 600 nm with a signal-to-background larger than 100 and external conversion efficiency of 40 %. We confirm that single photon purity and wavepacket interference are preserved during frequency conversion, and demonstrate that spectrally distinct QD emission lines can be converted to the same wavelength in the PPLN waveguide. The ability to use a single frequency conversion unit to erase spectral distinguishability in solid-state quantum emitters can be valuable in the development of scalable, chip-based photonic quantum information devices.

We thank Edward Flagg for information on volume Bragg gratings and Lijun Ma and Xiao Tang for discussions about PPLN waveguides. S.A. and I.A. acknowledge support under the Cooperative Research Agreement between the University of Maryland and NIST-CNST, Award 70NANB10H193.

* serkan.ates@nist.gov
† kartik.srinivasan@nist.gov

[1] P. Kumar, Opt. Lett. **15**, 1476 (1990).
[2] A. J. Shields, Nature Photonics **1**, 215 (2007).
[3] K. F. Reim, J. Nunn, V. O. Lorenz, B. J. Sussman, K. C. Lee, N. K. Langford, D. Jaksch, and I. A. Walmsley, Nature Photonics **4**, 218 (2010).
[4] N. Sangouard, C. Simon, J. c. v. Minář, H. Zbinden, H. de Riedmatten, and N. Gisin, Phys. Rev. A **76**, 050301 (2007).
[5] M. M. Fejer, G. A. Magel, D. H. Jundt, and R. L. Byer, IEEE J. Quan. Elec. **28**, 2631 (1992).
[6] A. H. Gnauck, R. Jopson, C. McKinstrie, J. Centanni, and S. Radic, Opt. Express **14**, 8989 (2006).
[7] J. M. Huang and P. Kumar, Phys. Rev. Lett. **68**, 2153 (1992).
[8] G. Giorgi, P. Mataloni, and F. De Martini, Phys. Rev. Lett. **90**, 027902 (2003).
[9] S. Tanzilli, W. Tittel, M. Halder, O. Alibart, P. Baldi, N. Gisin, and H. Zbinden, Nature **437**, 116 (2005).
[10] M. T. Rakher, L. Ma, O. Slattery, X. Tang, and K. Srinivasan, Nature Photonics **4**, 786 (2010).
[11] H. J. McGuinness, M. G. Raymer, C. J. McKinstrie, and S. Radic, Phys. Rev. Lett. **105**, 093604 (2010).
[12] R. Ikuta, Y. Kusaka, T. Kitano, H. Kato, T. Yamamoto, M. Koashi, and N. Imoto, Nature Communications **2** (2011).
[13] S. Zaske, A. Lenhard, C. A. Kessler, J. Kettler, C. Hepp, C. R. Albrecht, W.-M. Schulz, M. Jetter, P. Michler, and C. Becher, http://www.arxiv.org/abs/1204.6253 (2012).
[14] C. Kurtsiefer, S. Mayer, P. Zarda, and H. Weinfurter, Phys. Rev. Lett. **85**, 290 (2000).
[15] E. B. Flagg, A. Muller, S. V. Polyakov, A. Ling, A. Migdall, and G. S. Solomon, Phys. Rev. Lett. **104**, 137401 (2010).
[16] R. B. Patel, A. J. Bennett, I. Farrer, C. A. Nicoll, D. A. Ritchie, and A. J. Shields, Nature Photonics **4**, 632 (2010).
[17] R. Lettow, Y. L. A. Rezus, A. Renn, G. Zumofen, E. Ikonen, S. Götzinger, and V. Sandoghdar, Phys. Rev. Lett. **104**, 123605 (2010).
[18] H. Bernien, L. Childress, L. Robledo, M. Markham, D. Twitchen, and R. Hanson, Phys. Rev. Lett. **108**, 043604 (2012).
[19] A. Sipahigil, M. L. Goldman, E. Togan, Y. Chu, M. Markham, D. J. Twitchen, A. S. Zibrov, A. Kubanek, and M. D. Lukin, Phys. Rev. Lett. **108**, 143601 (2012).
[20] H. Takesue, Phys. Rev. Lett. **101**, 173901 (2008).
[21] M. Ghioni, A. Gulinatti, I. Rech, F. Zappa, and S. Cova, IEEE J. Sel. Top. Quan. Elec. **13**, 852 (2007).
[22] A. Gulinatti, I. Rech, F. Panzeri, C. Cammi, P. Maccagnani, M. Ghioni, and S. Cova, J. Mod. Opt. **59**, 1 (2012).
[23] K. Sanaka, A. Pawlis, T. D. Ladd, K. Lischka, and Y. Yamamoto, Phys. Rev. Lett. **103**, 053601 (2009).
[24] See supplementary material for details regarding experimental setups, measurements, and data analysis.
[25] K. Srinivasan and O. Painter, Nature (London) **450**, 862 (2007).
[26] C. K. Hong, Z. Y. Ou, and L. Mandel, Phys. Rev. Lett. **59**, 2044 (1987).
[27] C. Langrock, E. Diamanti, R. Roussev, Y. Yamamoto, M. Fejer, and H. Takesue, Opt. Lett. **30**, 1725 (2005).
[28] M. T. Rakher, L. Ma, M. Davanço, O. Slattery, X. Tang, and K. Srinivasan, Phys. Rev. Lett. **107**, 083602 (2011).
[29] J. S. Pelc, L. Ma, C. R. Phillips, Q. Zhang, C. Langrock, O. Slattery, X. Tang, and M. M. Fejer, Opt. Express **19**, 21445 (2011).
[30] H. Dong, H. Pan, Y. Li, E. Wu, and H. Zeng, Appl. Phys. Lett. **93**, 071101 (2008).
[31] C. Santori, D. Fattal, J. Vuckovic, G. Solomon, and Y. Yamamoto, Nature **419**, 594 (2002).
[32] A. Kiraz, M. Ehrl, T. Hellerer, O. E. Müstecaplıoğlu, C. Bräuchle, and A. Zumbusch, Phys. Rev. Lett. **94**, 223602 (2005).
[33] R. B. Patel, A. J. Bennett, K. Cooper, P. Atkinson, C. A. Nicoll, D. A. Ritchie, and A. J. Shields, Phys. Rev. Lett. **100**, 207405 (2008).
[34] A. Kiraz, S. Falth, C. Becher, B. Gayral, W. V. Schoenfeld, P. M. Petroff, L. Zhang, E. Hu, and A. Imamoglu, Phys. Rev. B **65**, 161303 (2002)
.

SUPPLEMENTARY INFORMATION

EXPERIMENTAL SETUPS

Figure 6 shows a detailed schematic of the experimental setup used for photon correlation and two-photon interference measurements before and after frequency conversion of a single QD state. The individual sub-systems within this setup are described below.

Quantum dot single photon source

Our source of single photons consists of an InAs quantum dot (QD) in a 190 nm thick, 2.9 μm diameter GaAs microdisk cavity. In this work, the coupling between the modes of the cavity and the QD emission lines is weak, and any radiative rate enhancement or inhibition is relatively small (< 2 X). QD emission is out-coupled from the microdisk cavity using an optical fiber taper waveguide (FTW), which provides a convenient single mode fiber interface for subsequent experiments. The sample is cooled in a liquid He flow cryostat, and a sample temperature between 7 K and 10 K is maintained during all experiments.

Spectral filtering of the QD emission

Emission that is out-coupled by the FTW is sent into a filtering setup consisting of a ≈ 0.2 nm bandwidth volume reflective Bragg grating (BPF in Fig. 6) whose input is coupled to single mode optical fiber and output is coupled to polarization maintaining (PM) single mode fiber. Quarter- and half-wave plates and a polarizing beamsplitter are placed prior to the PM fiber input, to ensure that light is linearly polarized along the slow-axis of the fiber. The typical throughput of the filtering setup is between 50 % and 60 %.

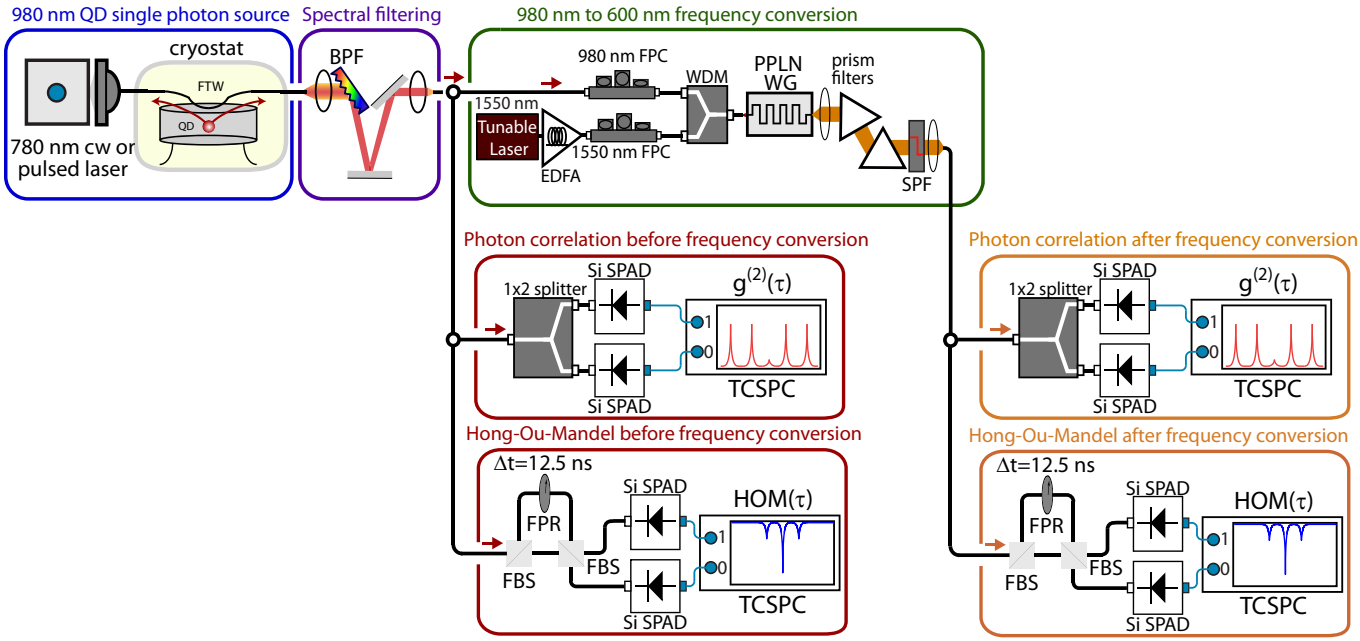

FIG. 6. (a) Detailed schematic of the experimental setups used within this work to demonstrate preservation of photon statistics and two-photon interference during frequency conversion from the 980 nm band to 600 nm. QD = quantum dot; FTW = fiber taper waveguide; BPF = bandpass filter; EDFA = erbium-doped fiber amplifier; FPC = fiber polarization controller; WDM = wavelength division multiplexer; SPF = short-pass filter; PPLN WG = periodically-poled lithium niobate waveguide; SPAD = single photon avalanche diode; FBS = fiber-coupled beamsplitter; FPR = fiber-coupled polarization rotator; TCSPC = time-correlated single photon counting board.

Frequency conversion

In the frequency conversion setup, we use a wavelength division multiplexer (WDM) to combine the spectrally-filtered QD emission with a strong (few hundred mW) 1550 nm pump signal that is generated by an external cavity tunable diode laser and erbium-doped fiber amplifier (EDFA). Fiber polarization controllers (FPCs) are used to adjust the polarization state of both the 980 nm and 1550 nm beams. The combined signal and pump are coupled into a 2 cm long, 5 % MgO-doped PPLN waveguide whose temperature can be adjusted between 25 °C and 90 °C with 0.1 °C resolution. Light is coupled into the waveguide through a cleaved single mode optical fiber that is controlled by a 3-axis open-loop piezo stage and has a mode-field diameter of 5.8 μm at 980 nm. The coupling is optimized for the 980 nm band signal, at the expense of the 1550 nm pump (additional pump power compensates for the 1550 nm coupling inefficiency). Light exiting the PPLN waveguide is collimated and sent through two dispersive prisms and two 750 nm short pass edge filters (SPFs) to eliminate residual 1550 nm pump photons and frequency doubled 775 nm pump photons from the signal. After filtering, the upconverted signal is usually coupled into a PM single mode fiber. We place a polarizing beamsplitter prior to the PM fiber output to ensure that light is linearly polarized along the slow-axis of the fiber (waveplates are not needed because the output of the PPLN waveguide is very close to linearly polarized).

The external conversion efficiency of the setup is as high as ≈40 %, including all losses in the system other than the final single mode fiber coupling, which has a typical efficiency of 30 %. In some experiments (i.e., ones in which the spatial mode profile of the light is unimportant), multimode fiber coupling is preferred, due to its higher coupling efficiency of 85 %. The overall detection efficiency of the frequency conversion system is given as the product of the external conversion efficiency, the fiber coupling efficiency, and detector quantum efficiency (≈ 67 % at 600 nm for a thick Si single-photon avalanche diode).

Si single-photon avalanche diode (SPADs)

Three different types of Si single-photon avalanche diodes (SPADs) are used in the experiments, depending on the requirements on detection efficiency and timing resolution. Thick Si SPADs used in this work have a detection efficiency of ≈12.5 % (67 %) at 980 nm (600 nm) and a timing jitter >500 ps, and are used in experiments in which high timing resolution are not needed. Thin Si SPADs [21] have a detection efficiency of ≈2 % (45 %) at 980 nm (600 nm), and a timing jitter of ≈50 ps. Newly-developed red-enhanced Si SPADs [22] have a detection efficiency of ≈6 % (55 %) at 980 nm (600 nm), and a timing jitter of ≈100 ps.

As evident from these efficiency and timing jitter values, an advantage of using frequency conversion to the 600 nm band is the potential to simultaneously achieve high quantum efficiency (> 40 %) and low timing jitter (≈ 50 ps), which is currently not possible in the 980 nm band using Si SPAD technology.

Pulsed photon correlation measurement

In pulsed measurements, the QD is pumped with a gain-switched 780 nm laser diode operating with a 50 MHz repetition rate and 50 ps pulse width. Prior to frequency conversion, spectrally-isolated QD emission is split using a 1x2 fiber splitter, and each output of the splitter is sent to a thick Si SPAD. The SPAD outputs are sent to a time-correlated single photon counting (TCSPC) system with a bin size of 512 ps, and histogram data is acquired to measure the second-order intensity correlation function $g^{(2)}(\tau)$.

Measurements after frequency conversion are performed in a similar fashion, with the output of the frequency conversion setup directed to a 1x2 fiber splitter, and subsequently, into thick Si SPADs and the TSCPC.

Continuous wave photon correlation measurement

Continuous wave (cw) measurements are performed in a manner similar to that used for pulsed measurements, with the following exceptions: (1) a 780 cw laser is used to excite the QD. (2) High timing resolution SPADs and a smaller TCSPC histogramming bin width are used. For measurements before frequency conversion, two red-enhanced Si SPADs are used, and the bin size of the TCSPC is set to 256 ps.

For measurements after frequency conversion, one red-enhanced Si SPAD and one thin Si SPAD are used, and the bin size of the TCSPC is set to 256 ps.

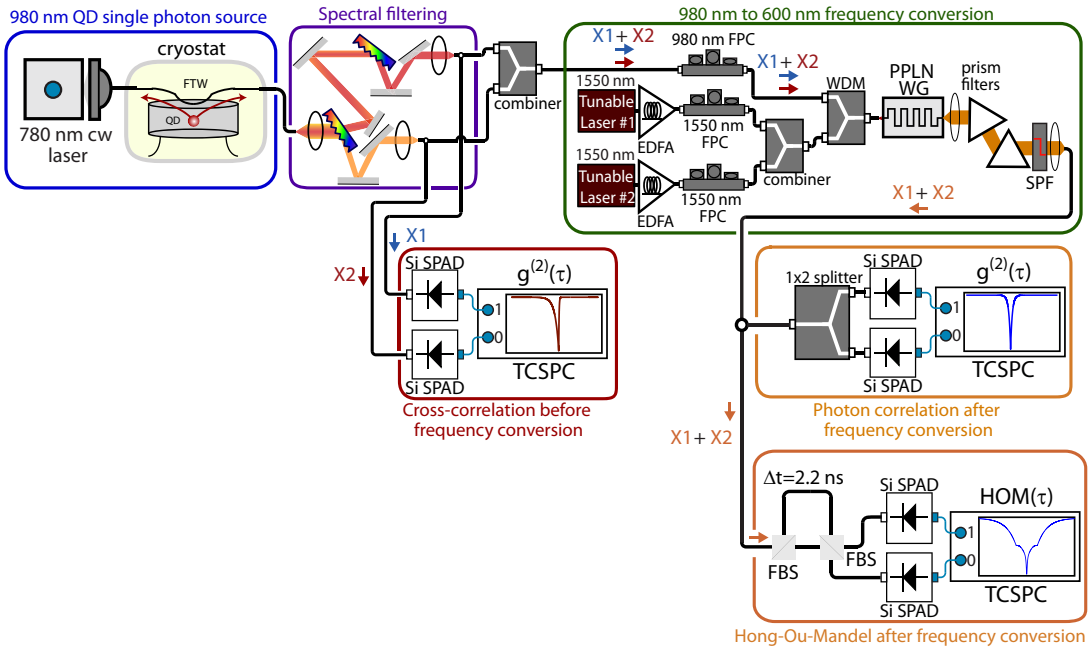

FIG. 7. Detailed schematic of the experimental setup used for frequency conversion of two spectrally-separated QD states to the same wavelength.

Single state two-photon interference measurement

Two-photon interference measurements are performed using Mach-Zehnder interferometers for the 980 nm band (before conversion) and 600 nm band (after conversion). Each interferometer starts with a PM-fiber-coupled beam-splitter (FBS in Fig. 6). One output of the FBS is connected directly into the first input port of a second FBS, while the other output goes through a fiber-coupled polarization rotator (FPR) before being connected to the second input port of the second FBS. The FPR can be rotated to allow both maximum interference (parallel configuration) or minimum interference (orthogonal configuration), and its input and output cables provide a delay of 12.5 ns with respect to the other arm of the interferometer.

For measurements done before frequency conversion, the outputs of the 980 nm band Hong-Ou-Mandel setup are detected with the two red-enhanced Si SPADs. For measurements after frequency conversion, one red-enhanced Si SPAD and one thin Si SPAD are used, and the outputs are sent to the TCSPC. Data is acquired in a time-tagged, time-resolved mode in which the photon arrival times from each channel are recorded with 4 ps timing resolution and the bin size set during subsequent data analysis. Here, a bin size of 125 ps was used for measurements before and after conversion.

Photon correlation measurements using two state frequency conversion

The experimental setup used for studying the frequency conversion of two spectrally-separate QD states is shown in Fig. 7. Prior to conversion, we perform cross-correlation measurements by spectrally isolating lines X1 and X2 using reflective volume gratings whose outputs are coupled to single mode optical fibers. The fibers are connected to red-enhanced Si SPADs, whose outputs are fed into the TCSPC. Data is acquired in time-tagged, time-resolved mode and a bin size of 50 ps was used in analyzing the data.

To frequency convert states X1 and X2 to the same wavelength in the 600 nm band, two 1550 nm band external cavity diode lasers are separately amplified and combined with lines X1 and X2 in the PPLN waveguide. Each 1550 nm laser is tuned to maximize the frequency conversion of the corresponding QD state, and the output of the PPLN waveguide is spectrally resolved to determine the precise wavelength to which light is converted. Fine tuning of the 1550 nm wavelengths is performed to ensure that both states are converted to the same wavelength (within the resolution of the grating spectrometer). This adjustment can come at the expense of conversion efficiency (in practice, we sacrifice on the conversion efficiency of state X1, since it is brighter).

The combined frequency converted light from states X1 and X2 is coupled into a single mode PM fiber and split using a 1x2 fiber splitter, with the arms of the splitter hooked up to a red-enhanced Si SPAD and a thin Si SPAD. Data is acquired in time-tagged, time-resolved mode and a bin size of 50 ps was used in the data analysis.

Two-photon interference measurement using two state frequency conversion

Two-photon interference of two QD states follows the same procedure as above, where both states are frequency converted to the same wavelength in a single PPLN waveguide. The combined frequency converted light from the two states is sent to a Mach-Zehnder interferometer (Fig. 7), and the outputs of the interferometer are hooked up to a red-enhanced Si SPAD and a thin Si SPAD. Data is acquired in time-tagged, time-resolved mode, and due to the relatively low photon count rates in this measurement (more details are given in the final section below), a bin size of 250 ps was used in analysis of the data.

MEASUREMENTS AND DATA ANALYSIS

Quasi-phase-matching response and temperature tuning

We measure the quasi-phase-matching bandwidth of the PPLN waveguide as follows. The weak signal produced by a narrow linewidth (<5 MHz) laser is fixed at 983.8 nm, and the temperature of the PPLN waveguide is set to 58.8 °C. Next, the 1550 nm pump power is set to ≈ 800 mW, close to the value at which we achieve optimal conversion efficiency. We then scan the 1550 nm pump wavelength while monitoring the frequency converted 600 nm band signal on a thick Si SPAD. This generates the plot shown in the inset to Fig. 1(b). We infer the 980 nm quasi-phase-matching bandwidth based upon energy conservation and the 1550 nm wavelengths.

Adjusting the temperature of the PPLN waveguide provides a mechanism to tune the output wavelength of the frequency conversion process. At each PPLN waveguide temperature, we keep the input signal fixed at 983.8 nm and scan the 1550 nm laser, recording the 1550 nm wavelength at which the conversion efficiency is maximized. Using this 1550 nm wavelength and the requirement of energy conservation produces the plot of frequency converted wavelength against temperature in Fig. 1(b).

Signal-to-background measurements

Signal-to-background measurements are performed using a thick Si SPAD placed after the prisms and SPFs, and with a 1550 nm band pump beam whose average power at the input of the 980/1550 nm WDM varies between 0 W and 1.2 W. The converted signal was measured using a weak 980 nm band input signal produced by an attenuated laser. The output average power level is set to be consistent with that of the QD single photon sources under investigation (≈30 fW), while the background level was determined by switching off the 980 nm laser. The dark count rate of the SPAD (≈50 s^{-1}) was subtracted from both the converted signal and background levels, to provide a metric that is independent of the characteristics of the detector. The error bars in Fig. 1(c) are one standard deviation values and are due to fluctuations in the detected count rate on the SPAD.

Lifetime measurements

Lifetime measurements reveal a radiative lifetime of $T_1 \approx 1$ ns for device M1, while devices M2 and M3 show longer lifetimes of ≈1.5 ns and 1.7 ns, respectively. These measurements are performed using the 780 nm pulsed laser, with the electronic trigger output of the laser fed to the first channel of the TCSPC, and the detected signal from a red-enhanced Si SPAD fed to the second channel.

$g^{(2)}(\tau)$ measurements

Measurement of the second-order correlation function $g^{(2)}(\tau)$ are performed using the setups described above. In pulsed measurements, the $g^{(2)}(0)$ value is determined by comparing the integrated area of the peak around time zero

to the average area of the peaks away from time zero. The uncertainty on this value is given by the standard deviation in the area of the peaks away from time zero. $g^{(2)}(\tau)$ under cw excitation is normalized to the coincidence rate at long time delays ($\tau > 500$ ns). The uncertainty in $g^{(2)}(0)$ is due to the fluctuation in coincidence rate for $\tau > 500$ ns, and is the one standard deviation value. Measurements are run for a long enough time for the Poissonian levels to reach a minimum of 80 coincidences.

Single state two-photon interference measurements

Two-photon interference experiments on device M2 are performed using the setups described above. The correlation functions at the output of the Mach-Zehnder interferometers under parallel and orthogonal polarizations of the photons, $g^{(2)}_{\parallel}(\tau)$ and $g^{(2)}_{\perp}(\tau)$, are normalized to the coincidence rate at long time delays ($\tau > 500$ ns). The uncertainties in $g^{(2)}_{\parallel,\perp}(0)$ are due to the fluctuations in the coincidence rate for $\tau > 500$ ns, and are listed as the one standard deviation value. Measurements are run for a long enough time for the Poissonian levels to reach a minimum of 100 coincidences.

To aid in the analysis of the two-photon interference data, we follow the procedure of Refs. 33 and 32. First, we consider that in the limit of no timing resolution limitations, the second-order correlation function $g^{(2)}(\tau)$ is of the form:

$$g^{(2)}(\tau) = 1 - \alpha e^{(-|\tau|/\tau_r)}, \tag{1}$$

where τ_r is the radiative lifetime of the QD state, and α accounts for potential multi-photon contributions to the data (i.e., that lead to a non-zero value of $g^{(2)}(0)$). The timing resolution of the SPADs and TCSPC are taken into account by convolving eq. (1) with the SPAD instrument response function and binning the result over a time window equal to the time bin set on the TCSPC.

Using the above approach, we fit the cw $g^{(2)}(\tau)$ data, as shown in the dashed lines in Fig. 3(a) and (d). The values we extract for α ($\approx$0.1) and τ_r ($\approx$1.5 ns) are then used with eq. (1) in formulas for $g^{(2)}_{\parallel}(\tau)$ and $g^{(2)}_{\perp}(\tau)$ [33]:

$$g^{(2)}_{\parallel}(\tau) = 4(T_1^2 + R_1^2)R_2T_2g^{(2)}(\tau) + 4R_1T_1[T_2^2g^{(2)}(\tau - \Delta\tau) + R_2^2g^{(2)}(\tau + \Delta\tau)](1 - ve^{-2|\tau|/\tau_c})), \tag{2}$$

$$g^{(2)}_{\perp}(\tau) = 4(T_1^2 + R_1^2)R_2T_2g^{(2)}(\tau) + 4R_1T_1[T_2^2g^{(2)}(\tau - \Delta\tau) + R_2^2g^{(2)}(\tau + \Delta\tau)], \tag{3}$$

R and T are the reflection and transmission intensity coefficients at the two beamsplitters, which we assume to be 0.5 for all of the beamsplitters in use. v is the spatial overlap of the photon wavepackets at the second beamsplitter, which we assume to be unity, and $\Delta\tau$ is the delay in the fiber-coupled Mach-Zehnder interferometer, which is $\approx$12.5 ns. Accounting for the timing resolution of the SPADs and TCSPC in the same way as described above for $g^{(2)}(\tau)$, we produce the dashed line curves shown in Fig. 3(b),(c) and (e),(f). The extracted coherence time $\tau_c = 100$ ps is consistent with independent measurements of coherence time for QDs under 780 nm excitation on this sample, which show a range of values between $\approx$75 ps and 250 ps.

Finally, the visibility of the two-photon interference is given by:

$$\mathrm{V} = (g^{(2)}_{\perp}(0) - g^{(2)}_{\parallel}(0))/g^{(2)}_{\perp}(0). \tag{4}$$

Two state two-photon interference measurements

Autocorrelation and cross-correlation data from states X1 and X2 of device M3 are shown in Fig. 8, and establish that both states come from the same QD. For the X1 and X2 autocorrelation, $g^{(2)}(0) = 0.10 \pm 0.02$ and $g^{(2)}(0) = 0.21 \pm 0.02$, respectively, while the X1-X2 cross-correlation has $g^{(2)}(0) = 0.11 \pm 0.02$. The difference in $g^{(2)}(0)$ values between X1 and X2 arises from the relative position of the two states with respect to a broad cavity mode, which is more closely aligned with state X2. This also influences the radiative lifetime of the two states, as clearly visible in the correlation data in Fig. 8.

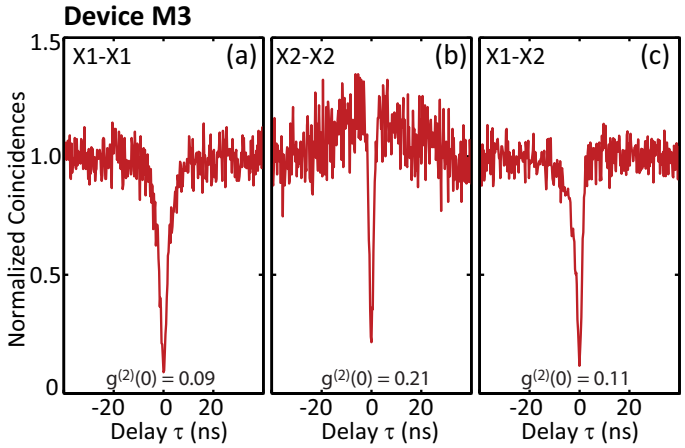

FIG. 8. Data for device M3 before frequency conversion. (a) Autocorrelation of state X1, (b) Autocorrelation of state X2, (c) Cross-correlation between states X1 and X2.

Two-photon interference of the frequency converted signal from the states X1 and X2 is performed using the 600 nm Mach-Zehnder interferometer (Fig. 7). To limit losses, the fiber-coupled polarization rotator is removed in the parallel polarization configuration (since the polarization is correctly aligned without it), and the resulting delay between the two arms of the interferometer is 2.2 ns. In addition, a bin size of 250 ps is used in analyzing the time-tagged, time-resolved data, which was acquired for 2.5 h to produce the data in Fig. 5(b)-(c).

The data is fit using the same approach as described in the single state two-photon interference section, but now with $\Delta\tau$=2.2 ns. Because $g^{(2)}(\tau = 2.2 \text{ ns}) < 1$ (in part due to the relatively long lifetimes of the states involved, with $T_1 \gtrsim 1.5$ ns), the value of $g^{(2)}(0)$ in the perpendicular polarization configuration, $g_{\perp}^{(2)}(0)$, can be less than 0.5, which is what one typically predicts for this non-interfering configuration in the case of a pure single photon source [33]. Non-zero multiphoton probability (i.e., $g^{(2)}(0) > 0$) will also influence $g_{\perp}^{(2)}(0)$. Our best estimates of $T_1 = 1.7$ ns, $g^{(2)}(0) = 0.1$, and τ_c=200 ps yield the red solid curve (parallel polarization configuration) and black dashed line (orthogonal polarization configuration) in Fig. 5(b). This gives $g_{\perp}^{(2)}(0) = 0.45 \pm 0.04$, and even if infinite timing resolution of the detectors and $g^{(2)}(0) = 0$ are assumed, $g_{\perp}^{(2)}(0) = 0.36$. The significant reduction measured in the parallel polarization configuration, with $g_{\parallel}^{(2)}(0) = 0.13 \pm 0.04$, is thus attributed to the two-photon interference effect.

Future improvements to the setup will likely require improved optical losses. Extra losses within the setup relative to the two-photon interference of a single QD state include: (1) The necessity to achieve precise spectral matching of the upconverted wavelength, which requires fine tuning of the two 1550 nm pump lasers away from the peak conversion wavelengths, (2) The limited 1550 nm band pump power available due to the directional coupler used to combine the two pump signals, which limits the power in any one pump field to $\approx$ 500 mW and prevents operation at the peak of the external conversion efficiency curve of Fig.1(c), and (3) The directional coupler used to combine the X1 and X2 emission after spectral filtering, which automatically adds 3 dB of loss due to the unused output port. Improvement in the losses of the fiber-coupled beamsplitters (>3 dB total) and the single mode fiber coupling at the output of the PPLN waveguide (5.2 dB) (also present in the single state two-photon interference experiment) would also help improve the signal-to-noise level in the measurements.